

pubs.acs.org/JPCC Article

In-Operando FTIR Study on the Redox Behavior of Sulfurized Polyacrylonitrile as Cathode Material for Li—S Batteries

Rhyz Pereira, Krishna Kumar Sarode, Ayda Rafie, Aaron Fafarman, and Vibha Kalra*



Cite This: https://doi.org/10.1021/acs.jpcc.3c03421



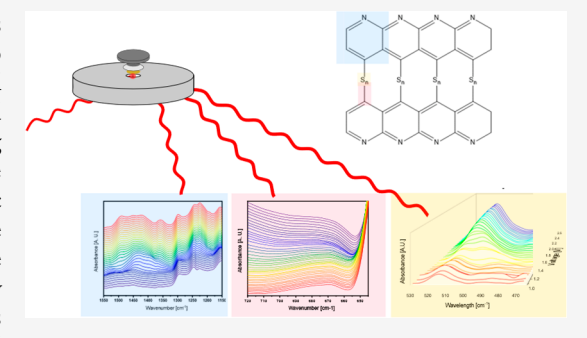
ACCESS

III Metrics & More

Article Recommendations

SI Supporting Information

ABSTRACT: Lithium—sulfur batteries have shown tremendous potential as a post lithium-ion battery chemistry, with a theoretical capacity of up to 1675 mAh/g. However, they have suffered from fundamental material challenges related to the insulating nature of the active material and discharge products as well as the solubility of intermediary products during the electrochemical reaction . One of the many proposed solutions to the latter problem has been to anchor the sulfur chain chemically to an organic molecule to form an organosulfur material. Sulfurized polyacrylonitrile (SPAN) is one such material that has shown tremendous promise. While SPAN has demonstrated long cycle life in carbonate electrolytes, its viability in ether electrolytes is only possible with the inclusion of high concentrations of lithium nitrate. To identify the chemical species present in charge and



discharge cycles, elucidate the mechanisms of capacity fade, and understand why capacity is retained in the presence of lithium nitrate, we combined post-mortem analysis by XPS with an in-operando FT-IR study of three spectral regions. We probed bond vibrations we have assigned to the carbon—sulfur bond that anchors sulfur chains to the organosulfur backbone, the sulfur—sulfur bond in lithium polysulfides that evolve in electrolyte, and ring stretches of the heteropolycyclic cyclized-PAN backbone. We present evidence in support of lithiation of the heteropolycyclic backbone. We identify the formation of a robust cathode—electrolyte interphase to be a critical feature of systems with lithium nitrate present. This allows for the retention of the C–S bond and the suppression of polysulfides that otherwise cause shuttling losses.

INTRODUCTION

Lithium-sulfur batteries have for the past decade shown great potential, promising capacities up to ~1675 mAh/g, and a cheap, abundant, and environmentally friendly active material. However, commercialization has remained out of reach due to several hurdles yet to be overcome. These include the insulating nature of the initial material (S₈) and the discharge product, lithium sulfide (Li₂S), volume expansion, and most importantly the polysulfide shuttle. 1,3,4 During the redox process, sulfur undergoes a complex chemical transformation, going from solid elemental sulfur to lithium polysulfides, which are soluble in the most widely used ether-based electrolytes. The soluble nature of polysulfides has posed enormous challenges to researchers in the field. These polysulfides shuttle via diffusion and migration processes to the anode where they irreversible react and lead to the loss of active material. 1,4-6 Over time, the loss of active material and the corrosion of the metal anode surface lead to battery failure. Numerous solutions have been proposed including porous cathode designs, trapping via electrostatic interactions, separator and interlayer modifications, and new electrolyte formulations.

One of the most promising cathode material solutions has been the sulfurization of polymeric structures to anchor polysulfide chains via covalently bound sulfur. Of these materials in development, one of the most studied has been sulfurized polyacrylonitrile (SPAN). SPAN has demonstrated excellent performance and compatibility with commercial carbonate electrolytes. SPAN's compatibility with carbonate electrolytes stands in contrast to traditional lithium-sulfur cells which exhibit adverse side reactions between polysulfides and carbonate electrolyte species, which render the cell inoperable within the first few cycles.8 SPAN, however, does not exhibit these side reactions, and it is thought that the bound polysulfides are incapable of adversely reacting with electrolyte species, and small molecular sulfur is protected by the polymeric matrix. However, SPAN's performance in etherbased electrolytes raises questions about this explanation. In ether-based electrolytes, SPAN cathodes begin to exhibit behavior similar to that of normal Li-S cells after several cycles. Ether-based electrolytes, despite their shortcomings, still offer advantages particularly in regard to the performance

Received: May 21, 2023
Revised: September 8, 2023



of the lithium metal anode. Anode stability, a less prominent concern in typical lab scale coin cells, becomes a major bottleneck during scale-up. 10 Ether-based cells typically exhibit more stable anode behavior, due in part to a more robust SEI layer compared to their carbonate counterparts. 11 However, the failure of SPAN cells in ether electrolytes and their reversion to typical Li-S behavior calls into question our understanding of the redox behavior of SPAN and, more broadly, that of sulfurized polymer compounds. In-situ studies are scarce and have typically been performed using Raman spectroscopy. Additionally, they have focused on SPAN cells using carbonate electrolyte and polysulfide formation and suppression. 12-14 Unique aspects of SPAN's chemical structure such as its polycyclic backbone have never been fully investigated using in-situ spectroscopy, despite computational and ex-situ evidence that the lithiation process plays an important role in the initial cycle. Non-carbonate-based studies are also sorely lacking despite ether-based cells demonstrating behavior that runs contrary to that of its carbonate counterparts. Wu et al. performed studies using spatially resolved postmortem X-ray absorption spectroscopy combined with ex-situ X-ray fluorescence (XRF) microscopy, X-ray photoelectron spectroscopy, and scanning electron microscopy on SPAN cells with ether electrolytes and managed to achieve stable cycling by increasing the concentration of lithium nitrate salt.² This study and other ex-situ studies have shown that a crystalline cathode-electrolyte interface (CEI) is integral in suppressing polysulfide dissolution and is composed of a layer LiF and LiNO₂ formed by introducing LiNO₃. 15

Indeed, a quasi-solid to solid conversion reaction has been proposed to explain SPAN's polysulfide mitigation ability, where S_8 is directly converted to $\text{Li}_2\text{S.}^{16}$ The control of interface conditions has been thought to be integral to this process, and a robust CEI layer would lead to such a phenomenon.¹⁶ For a solid-to-solid conversion to occur in such a manner, the sulfur atom must be fully surrounded by lithium ions and cannot interact with solvent species. However, the role that the carbon-sulfur bond plays in this is still not properly understood. The underlying assumption has been that it must play a major role in sulfur immobilization via covalently bound sulfur, despite conflicting evidence regarding the stability of this bond. 17,18 The aforementioned in-situ Raman studies have been inconclusive about the redox activity of the carbon-sulfur bond in SPAN. Other reports have performed ex-situ, computational, and electrochemical investigations have found that the C–S bond can be active during cycling, ^{19,20} and they have also found that it can be inert during cycling. ^{21–23} In previous work we demonstrated that the formation of loose polysulfides is inevitable in sulfur-rich copolymers above a certain sulfur percentage in ether electrolytes due to the cleavage of S-S bonds in long sulfur bridges resulting in capacity fade overtime.²⁴ If the carbon-sulfur bond remains stable during cycling or reforms, it could have a role in trapping polysulfides in the polymeric matrix leading to shielding of polysulfides from solvent species, preventing the dissolution and subsequent polysulfide shuttle, and exhibiting the quasi-solid to solid single plateau conversion that is observed.16

In this work, we endeavor to understand the redox behavior of SPAN using in-operando FTIR. SPAN's reported behavior in ether electrolytes leads us to hypothesize that the C-S bond is unstable and leads to the formation of soluble polysulfides. However, SPAN's larger voltage window, as well as SPAN's

behavior in electrolytes with high lithium nitrate concentrations, leaves many questions unanswered regarding the structural changes SPAN undergoes during cycling and the implications those changes have on cycling stability. In order to investigate these changes, we performed in-operando FTIR spectroscopy on Li-SPAN batteries coupled with post-mortem XPS. We observed the effects of high lithium nitrate concentrations on cycling stability and the formation of polysulfides therein, the stability of the C–S bond, and the structural changes the cyclized polymer backbone underwent. In doing so, we developed a more comprehensive understanding of SPAN as a cathode material in ether electrolytes and, more generally, the use of sulfurized polymers.

EXPERIMENTAL METHODS

SPAN Synthesis and CNF Fabrication. SPAN was synthesized by taking PAN powder (Sigma-Aldrich; $M_{\rm w}$: 150000) and elemental sulfur powder (Sigma-Aldrich, 100 mesh) in a 1:4 ratio and grinding in a mortar and pestle for approximately 1 h. In order to ensure complete homogenization, ball milling was performed for approximately 12 h at 400 rpm in the presence of ethanol. The fully homogenized mixture was then reacted in a tube furnace (Thermolyne) at 350 °C with a heating rate of 2 °C/min for 3 h under a constant flow of nitrogen gas. The reaction yielded a black SPAN powder that was used to fabricate the slurries for cycling and in-situ observations.

Carbon nanofiber (CNF) mats were fabricated as detailed in previous papers. In short, 10 wt % PAN was completely dissolved in *N,N*-dimethylformamide (DMF, Sigma-Aldrich). This solution was then electrospun after being loaded into a syringe with a 22-gauge needle. Electrospinning was performed with a flow rate of 0.2 mL/h with a syringe pump (New Era Pump Systems, Inc.), a distance of 15 cm between the needle and the current collector, and an applied voltage of 8–10 kV varied to ensure a smooth and beadless mat. Humidity inside the chamber was maintained at <20%, and the mats were spun for ~6 h. Mats were stabilized in air at 280 °C for 6 h followed by carbonization under continuous nitrogen flow at 1000 °C for 1 h in a tube furnace with a heating and cooling rate of 3 °C/min. The resultant CNF mats were then punched with 11 mm punches to form the freestanding cathodes.

Cell Fabrication and Electrochemical Testing Procedures. Slurry cathodes were made by taking the synthesized SPAN, carbon black, sodium carboxymethylcellulose (CMC), and styrene-butadiene (SBR) in a ratio of 80:10:5:5 and grinding in a water-based slurry and casting. The slurry was ground in a mixer (Flacktek) for 20 min at 3500 rpm. Slurries were cast by using a blade coater with a thickness of $\sim 50 \ \mu m$. The cathodes for the in-operando cell were prepared by dispersing the SPAN powders (10 wt %) in acetone via sonication for 1 h and drop-casting the appropriate amount of the suspension on to the CNF scaffold and drying for ~1 h at 140 °C. Other methods of SPAN integration such as melt diffusion and on-site synthesis were found to be inappropriate due to SPAN's properties. These CNF-SPAN cathode's electrochemical behavior was checked in coin cells to make sure they matched with the behavior of the slurries previously tested. The CV scans of these coin cells are provided in the Supporting Information (Figure S1). We observed behavior similar to that of the slurry cathodes, with similar first discharges followed by two-plateau behavior in the coin cells

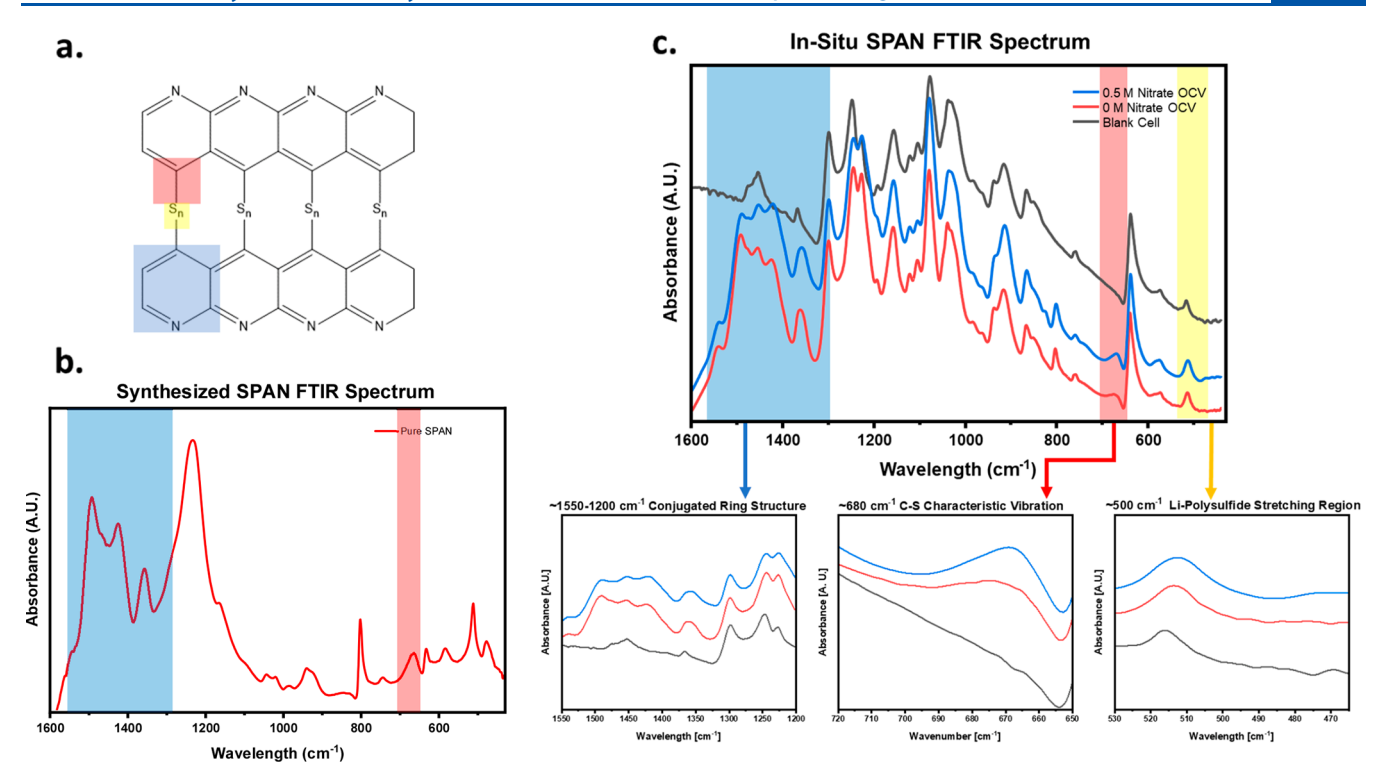


Figure 1. (a) Chemical structure of SPAN. (b) FTIR spectrum of SPAN after synthesis. (c) FTIR spectrum of SPAN in the in-situ cell assembly, with blank cell spectrum for reference; cell containing electrolyte with nitrate is shown in blue and without nitrate in red. Regions of interest are highlighted and zoomed in.

without nitrate and the single-plateau behavior in coin cells with nitrate.

The electrolyte was made by mixing 1,2-dimethoxyethane (DME, Alfa Aesar) and 1,3-dioxolane (DOL, Sigma-Aldrich) in a 1:1 volume ratio and dissolving 1 M lithium bis(trifluoromethanesulfonyl)imide (LiTFSI, CF₃SO₂NLiSO₂CF₃). To make electrolyte with lithium nitrate, an additional 0.5 M lithium nitrate (LiNO₃) was dissolved in the electrolyte. All cells and electrolyte were fabricated in an air-free glovebox. Coin cells were fabricated with 20 µL of electrolyte. Cycling was performed in a Neware cycler with galvanostatic chargedischarge experiments in the Li-SPAN voltage window of 1-3 V (vs Li/Li⁺). The cyclic voltammetry (CV) measurements were performed by using a Gamry (reference 1000) potentiostat. Cycled cells were then decrimped in the glovebox, and the cathodes were transferred to the XPS (PHI VersaProbe 5000) chamber via an air-free transfer cell to ensure no undesirable reactions would occur.

In-Operando FTIR Cell Assembly. To build the inoperando FTIR cell, we transferred the ATR puck into the argon-filled glovebox, and the coin cell assembly was replicated on the extended range diamond crystal. For this cell we used $45~\mu L$ of electrolyte, the cathode, a Celgard separator, and a Li metal anode (10 mm disc). The stainless-steel spacer was replaced with layered Ni foam (MTI Co.). The cell was sealed using a coin cell top, vacuum grease, and Kapton tape. The inoperando cell was then transferred outside the glovebox and connected to a Gamry reference 3000 potentiostat. The stainless-steel puck was used as the current collector for the cathode, and an Al foil strip was attached to the top of the coin cell to connect the in-operando cell to the Gamry potentiostat. We used the pressure anvil on the FTIR instrument to apply pressure to the cell and ensure a good contact inside the cell.

For collecting CVs, we first rested the cell for 1 h at its open-circuit potential. The CVs were collected with a scan rate of 0.02~mV/s between 1.0~and~3.0~V (vs Li/Li⁺) for three cycles. The collected series were then analyzed using macros in the Omnic software package, and each spectrum was corrected using background, baseline, and advanced ATR correction.

■ RESULTS AND DISCUSSION

SPAN Characterization and Electrochemical Behavior. SPAN was synthesized by milling polyacrylonitrile with elemental sulfur and heating to 350 °C for 3 h under nitrogen flow. Current literature hypothesizes that during the synthesis $-S_x$ - fragments covalently bond with C-C in the PAN backbone; 25,26 simultaneously dehydrogenation and cyclization forms polycyclic nitrogen heterocyclic ring structures along the PAN backbone and the evolution of H₂S (Figure 1a). These features are quite prominent in the FTIR spectrum. As highlighted in red in Figure 1b, the C-S bond that forms between elemental sulfur and PAN can be observed at 668 cm⁻¹. The peaks that occur between 1500 and 1200 cm⁻¹ are assigned to the aromatic heterocyclic ring and are highlighted in blue. These major features confirm the dehydrogenation, cyclization, and sulfurization of PAN to SPAN. Elemental analysis of the synthesized material showed a sulfur content of \sim 51–53% (Table S1). The SPAN was used as synthesized; extraction via carbon disulfide by stirring for ~48 h does demonstrate that ~2.8% of the sulfur is "loose" and can be dissolved away. The synthesis was confirmed to be successful by observing the FTIR spectra of the material and comparing to published reference spectrum of SPAN.²⁰ The initial electrochemical performance of the synthesized material was then confirmed via coin cell cycling (Figure 2a). Slurries were made by taking 80% SPAN, 10% carbon black, 5% sodium

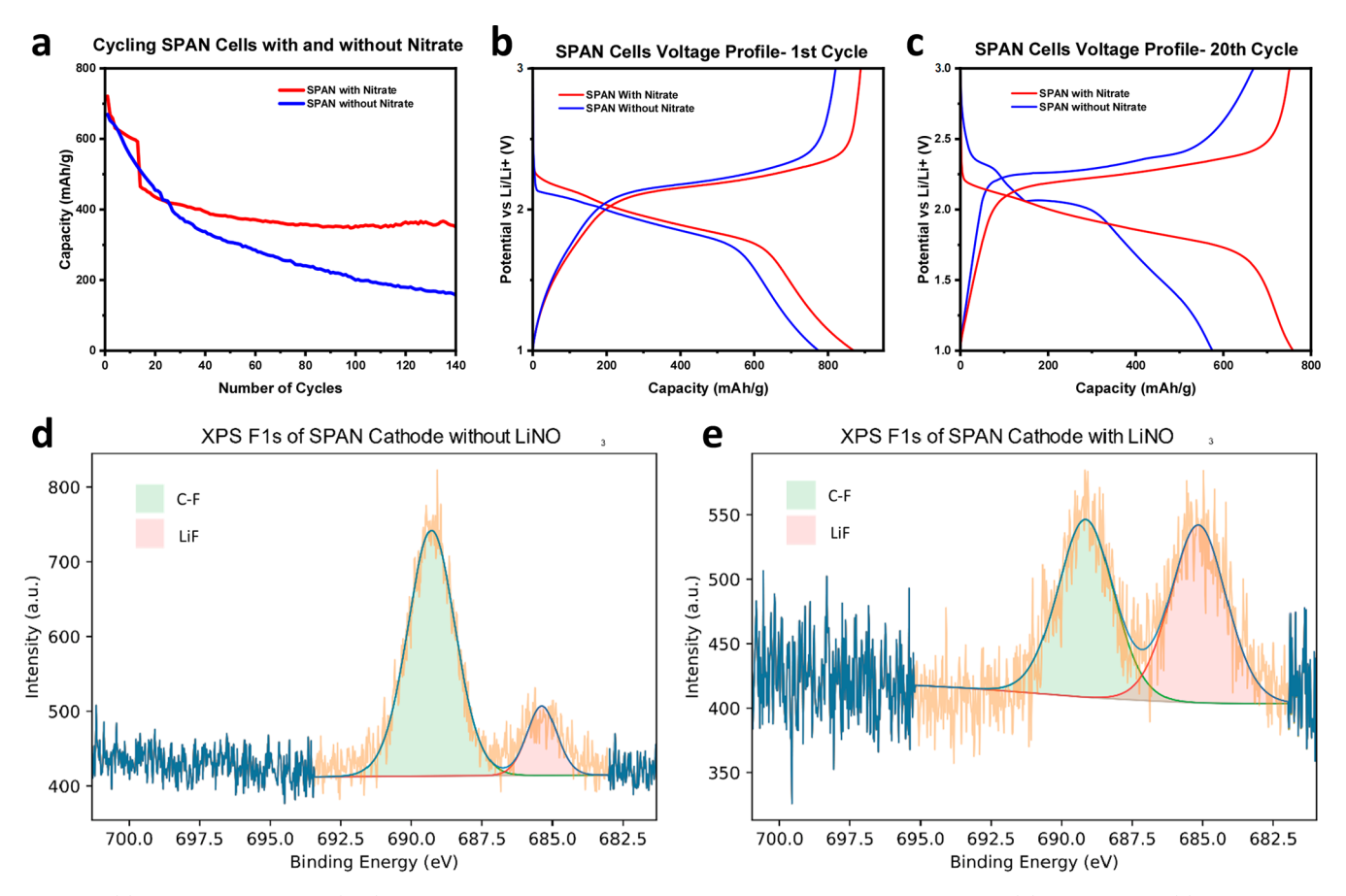


Figure 2. (a) Cycling stability and (b, c) voltage profiles of SPAN coin cells with and without nitrate after the (b) 1st cycle and (c) after the 20th cycle; voltage plateaus at 2.3 and 2.1 V emerge in cells without lithium nitrate after cycling. F 1s XPS spectra were taken after cycling for 10 cycles and demonstrate significantly smaller proportions of LiF (red fitted peak) vs C-F (green fitted peak) in cells without lithium nitrate (d) and cells with lithium nitrate (e).

carboxymethylcellulose (CMC), and 5% styrene—butadiene (SBR) grinding in a water-based slurry and casting. Two sets of electrolytes were created for these coin cells: one without lithium nitrate and one with lithium nitrate. The electrolyte was formulated by taking DOL and DME in a 1:1 volume ratio and adding 1 M lithium triflate. Lithium nitrate was added to the electrolyte at a concentration of 0.5 M. As seen in Figure 2a, the cells without lithium nitrate exhibit rapid capacity fade.

As seen in Figure 2b,c, the voltage profiles of the cycled coin cells reveal that both high concentrations of lithium nitrate and no lithium nitrate exhibit similar behavior in their first cycle. Various explanations for the large unrecoverable capacity of SPAN have been proposed, from lithium intercalation into the PAN structure to the permanent cleavage of the C-S bond. 12,18,26,27 Jin et al. using solid-state NMR found that the partially reversible lithiation of the SPAN backbone led to the large initial capacity, whereas Fanous et al. attributed the high irreversible initial capacity to cleavage of C-S bonds. 18,23 In any case, the behavior of the two electrolytes during cycling rapidly diverges after the first cycle. By the fifth cycle, cells with electrolytes that do not contain lithium nitrate start to exhibit two plateau behaviors, indicative of polysulfide formation and dissolution in the ether. This has been well-documented in ether electrolytes for conventional lithium-sulfur batteries with S_8 as the active material. The reduction of S_8 cleaves S– S bonds and forms soluble intermediate polysulfides (Li₂S_x) that can shuttle and cause capacity fade. Decrimped cells after

cycling also exhibit the distinctive yellow color of LiPSs, indicating that the polysulfide evolution does take place (Figure S6). The characteristic voltage plateau for this is observed at 2.3 V. In contrast, however, the electrolyte containing 0.5 M lithium nitrate does not exhibit this behavior; instead, single-plateau behavior is maintained while cycling while still maintaining higher capacities than the non-nitrate counterpart after the first irreversible loss (Figure 2a). Faster cycling at C/2 demonstrated that even after 100 cycles, singleplateau behavior is maintained. Wei et al. had demonstrated that cells with typical concentrations of lithium nitrate (~1% LiNO₃) demonstrated capacity fade in ether-based electrolytes.²⁸ The lack of any significant voltage plateau at 2.3 V at higher concentrations without any significant capacity tradeoffs is indicative of the presence of some mechanism to prevent the solubility of intermediate polysulfide species.

High concentrations of lithium nitrate have previously been found to suppress the polysulfide shuttle in SPAN cells, and a possible explanation for the single-plateau behavior has been the formation of a robust cathode—electrolyte interlayer (CEI).² These experiments found that electrolyte with lithium nitrate has a large reduction peak at \sim 1.5 V, indicating that this additive is not stable in the voltage window, in agreement with literature. For this reason, the voltage window of traditional lithium sulfur cells is confined to >1.8 V to prevent the decomposition of electrolyte species. Interestingly, despite the decomposition of lithium nitrate in the first cycle stable cycling

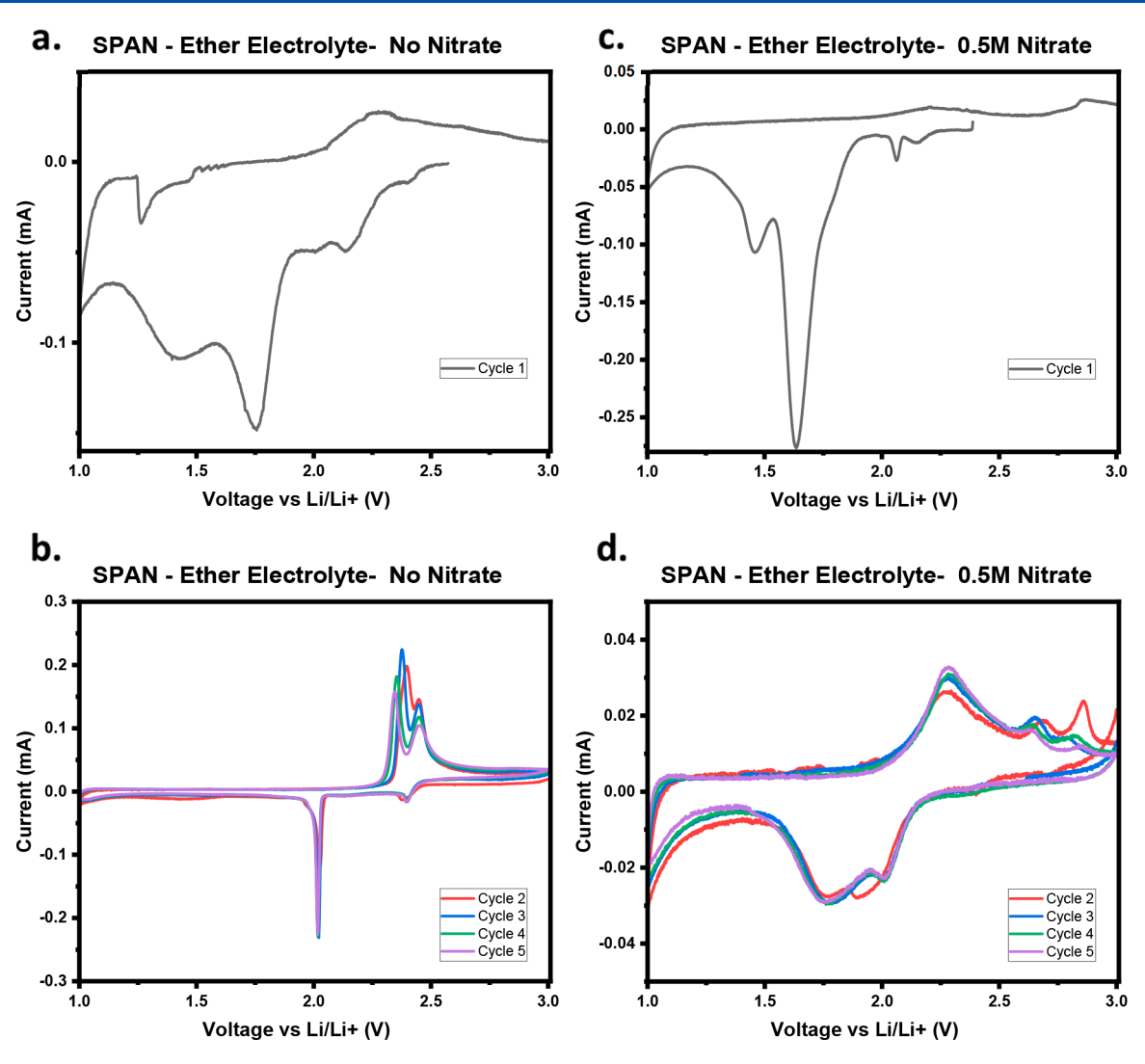


Figure 3. Cyclic voltammetry profiles of cells with and without nitrate. Profiles diverge in behavior following the first cycle, with prominent redox peaks at \sim 2.03 V associated with polysulfides in electrolyte without nitrate.

persists. This phenomenon leads us to believe that the presence of lithium nitrate alone does not suppress the shuttle effect, but rather the formation of degradation and side products contributes to shuttle suppression. Previous studies have found the synergistic effect of lithium nitrate and lithium polysulfide, together they facilitate the formation of a robust SEI layer on lithium metal. ^{29,30} The major component of these SEI's in high salt concentration electrolytes has been found to be lithium fluoride and lithium nitrite. 15 Other studies have also posited that the presence of lithium sulfate could contribute to the CEI layer.³¹ Qin et al. posit that sulfates could form because of parasitic side reactions that over the course of cycling lead to capacity loss. An examination of the post-mortem S 2p XPS spectrum (Figure S7) demonstrates that SPAN cathodes that were cycled for five cycles in electrolyte with and without nitrate both demonstrate high concentrations of lithium sulfate. This implies that a potential mechanism of the CEI layer could be the prevention of the parasitic side reactions during long-term cycling in addition to preventing polysulfide shuttle. Additionally, it demonstrates that oxidation via nitrate is not the only pathway in any potential parasitic reaction; parasitic pathways can arise from other oxygen-containing species in the electrolyte, such as the

ether electrolyte itself or trace impurities. As discussed above in Figure 2d,e, XPS shows a higher concentration of LiF on the surface of cathodes with high concentrations of LiNO₃. This provides strong evidence that the presence of a robust CEI contributes to the single-plateau behavior of the SPAN cathode by preventing the dissolution of intermediate polysulfides into the electrolyte. This fluorination of lithium is also exhibited in the C 1s XPS spectrum (Figure S9) where the electrolyte with nitrate has peaks associated with the C-F bond significantly suppressed in comparison to their no nitrate counterpart. In addition to LiF the post-mortem O 1s XPS (Figure S8) also exhibits Li₂O and Li₂O₂ on the cathode surface in cells that used electrolyte with high nitrate content, species that are not present at all in cells without nitrate. Indeed, cells without nitrate exhibited more oxygen bound to carbon. This implies that a robust cathode-electrolyte interface must be composed of inorganic lithium fluoride and lithium oxide species. However, major questions regarding the redox behavior of SPAN and the chemical transformations it undergoes while cycling remain unclear. To address the shortcomings of ex-situ studies, we performed in-situ measurements to observe the chemical transformations occurring in SPAN while undergoing redox.

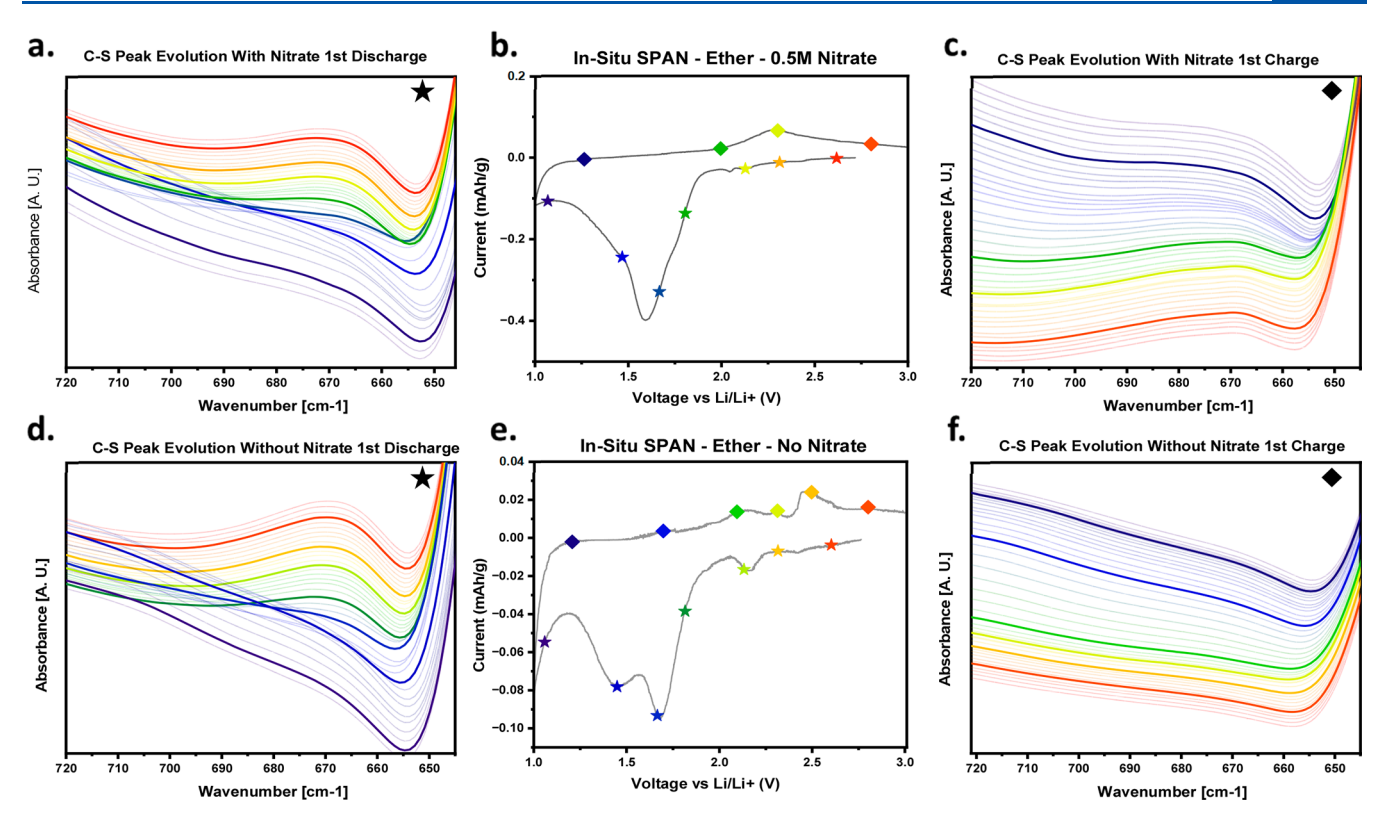


Figure 4. In-situ IR observations of the C–S region. The C–S peak disappears during the first discharge in both electrolytes with lithium nitrate (a) and without lithium nitrate (d), subsequently reappears in electrolyte with nitrate (c), and does not reappear in electrolyte without nitrate (f). The in-situ CV curves are provided in (b, e), and spectra of particular interest are marked and highlighted in the discharge curve with a star and charge curve with a diamond.

In-Situ IR Observation of the C-S Region. To get a better understanding of the mechanism underlying SPAN's redox behavior, we performed in-situ FTIR spectroscopy on the synthesized SPAN material. Our laboratory has previously designed an in-operando cell that has two important and unique features. The first one is the ATR accessory used, which also acts as a positive current collector. The second feature is the freestanding carbon nanofiber (CNF) mat used as a sulfur host, which does not require the addition of binders and can be used without the Al current collector, which would otherwise block the IR and prevent spectra collection. CNFs were infiltrated with SPAN; this architecture was tested in traditional coin cells, and the behavior matched the electrodes as prepared via slurry. Blank cell studies were conducted in both electrolytes using only the CNF scaffold without any active SPAN material as reference. Figure 1c shows the IR plots of the assembled cells containing SPAN, with nitrate, without nitrate, and blank cells without any SPAN present at OCV.

An important feature of SPAN is the C-S bond, which has been thought to play an important role in the suppression of soluble polysulfides, anchoring sulfur to a polymeric backbone. Many reports have shown, however, that this bond is not stable during cycling and is cleaved, contributing to the large initial discharge capacity in SPAN cells, which fades in subsequent cycles. However, conflicting information has been presented in regard to the possible reformation of this bond. Using in-situ IR, we can observe the C-S vibration at 670 cm^{-1,32} Over the course of charging and discharging in electrolyte without nitrate, we found that the peak assigned to the C-S vibration completely disappears (Figure 4d). A survey

of the difference spectrum ("fully discharged" minus "fully charged") 100 wavenumbers above or below the initial peak does not reveal any new peaks, ruling out the possibility of the peak merely shifting to a new frequency. The disappearance occurs at a discharge potential of 1.66 V, which corresponds well to the prominent reduction peak that is observed during the first discharge. This potential is also well below that of sulfur's reduction potential at 2.3 and 2.1 V. The C-S peak never recovers during the subsequent charge cycle in the cell with no nitrate additive (Figure 4f). Interestingly, while similar behavior is observed in cells with high concentrations of lithium nitrate during the initial discharge (Figure 4a), the subsequent charge cycle reveals a slight recovery of the C-S peak (Figure 4c). These observations coupled with the detection of a CEI (in nitrate-based cells) via our postmortem XPS discussed above lead us to hypothesize that the partial reversibility of the C-S bond breakage is due to the CEI preventing migration of polysulfide species away from the carbon backbone, thus maintaining an appreciable local sulfide concentration. In contrast, a lack of a robust CEI in the absence of nitrate cells permits polysulfide shuttle. In summary, we propose that CEI never allows sulfur molecules to fully solvate and allows for the reformation of C-S bonds to take place due to the presence of sulfur atoms near the cathode surface. In the case of Li-SPAN with carbonate electrolyte, C-S bond reversibility or partial reversibility has been evidenced by in-operando Raman studies. A study by Wang et al. claims that the C-S bond cleavage is reversible, 13 and one performed by Huang et al. found that cleavage is only partially reversible.¹² We note that these cells also have CEI formation due to the reaction of carbonate with small sulfur species. 15

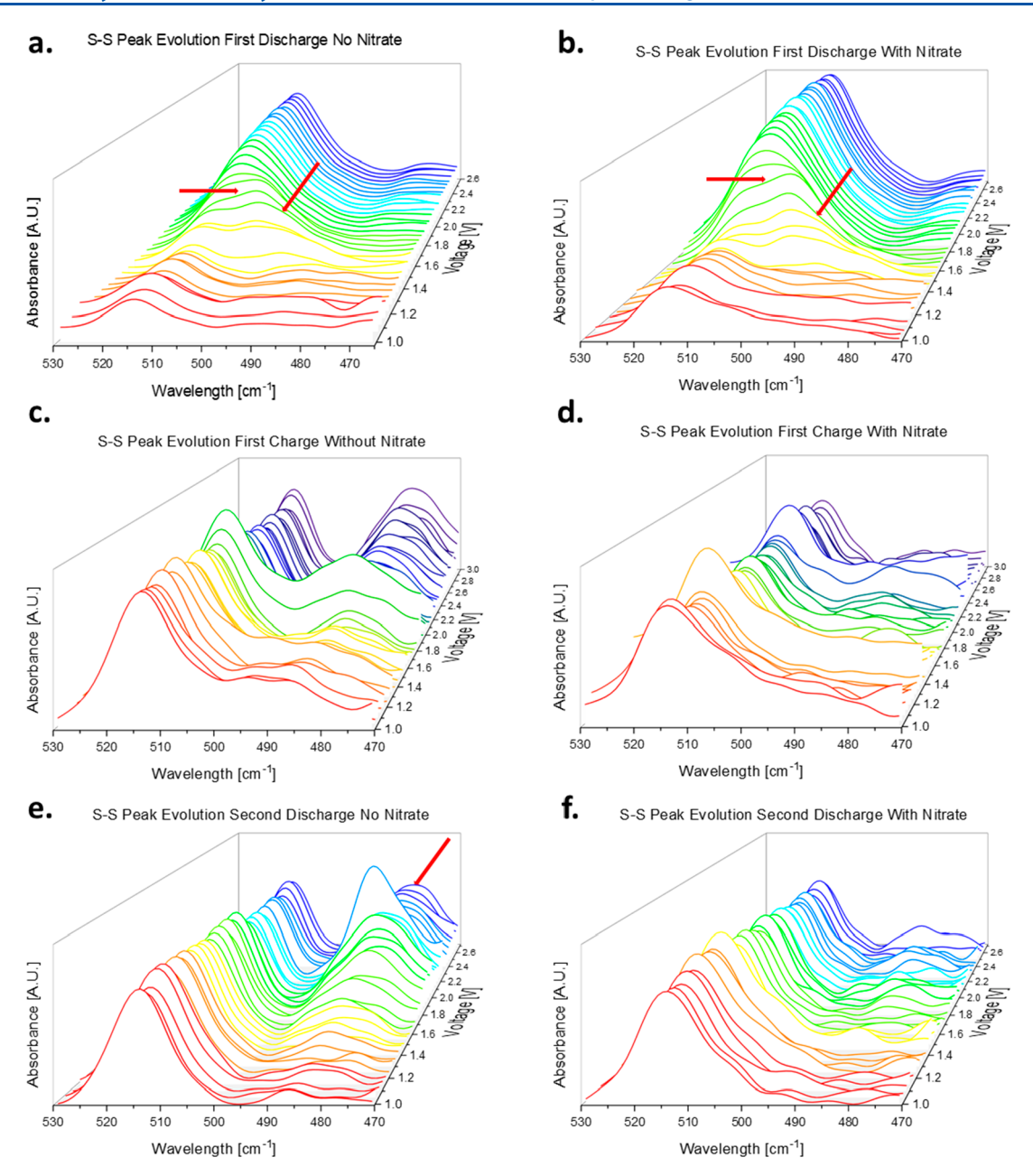


Figure 5. In-situ spectra of the S–S region for (a) first discharge with no nitrate, (b) first discharge with nitrate, (c) first charge without nitrate, (d) first charge with nitrate, (e) second discharge with no nitrate, and (f) second discharge with nitrate. Arrows provide locations for long-chain S–S bonds (a, b) and short-chain S–S bonds (e).

Thus, our hypothesis that the CEI is critical to reversible C-S bond formation is both novel and, to our understanding, generalizable.

In-Situ IR Observation of the S–S Region. The S–S bond stretching region was simultaneously interrogated to understand the speciation of the polysulfides over the charge/discharge cycle and the mechanism by which nitrate might be mitigating their formation. The lack of a prominent 2.3 V plateau in coin cells containing nitrate indicated that polysulfides were suppressed in some fashion. In our previous work, we showed that the IR peaks for lithium polysulfides are seen in the 480–510 cm⁻¹ window depending on the chain length. ^{24,33} Prior to discharge, there is a prominent absorbance band associated with the –CF₃ bending mode from the TFSI salt at 515 cm⁻¹, and this peak tends to get convoluted with long chain polysulfides which can appear as a shoulder to this

peak. We can observe this in the ~1.7 V trace in the first discharge (Figure 5a,b) at ~505 cm⁻¹ corresponding well with the height of the initial discharge peak in the CV measurements (Figure 1a,b). As the reduction reaction proceeds, this shoulder evolves into a distinct peak and gradually red-shifts to lower wavenumbers. This red-shift is typically associated with shorter chain polysulfides: 495 cm⁻¹ with S_6^{2-} , 490 cm⁻¹ with S_5^{2-} , and 485 cm⁻¹ with S_4^{2-} .³³ Interestingly, in the in-situ spectra, it was found that the polysulfide peaks occur in both the electrolyte with nitrate and the electrolyte without nitrate during the first cycle. We propose that some "unbound sulfur", that is, sulfur not bonded to carbon but rather bonded to other sulfur atoms, will still produce polysulfides that can be solvated into the electrolyte during the initial discharge. In the CVs, this appears as two slight blips at 2.1 V during the initial discharge. Starting from the first charge cycle, the behavior of the two

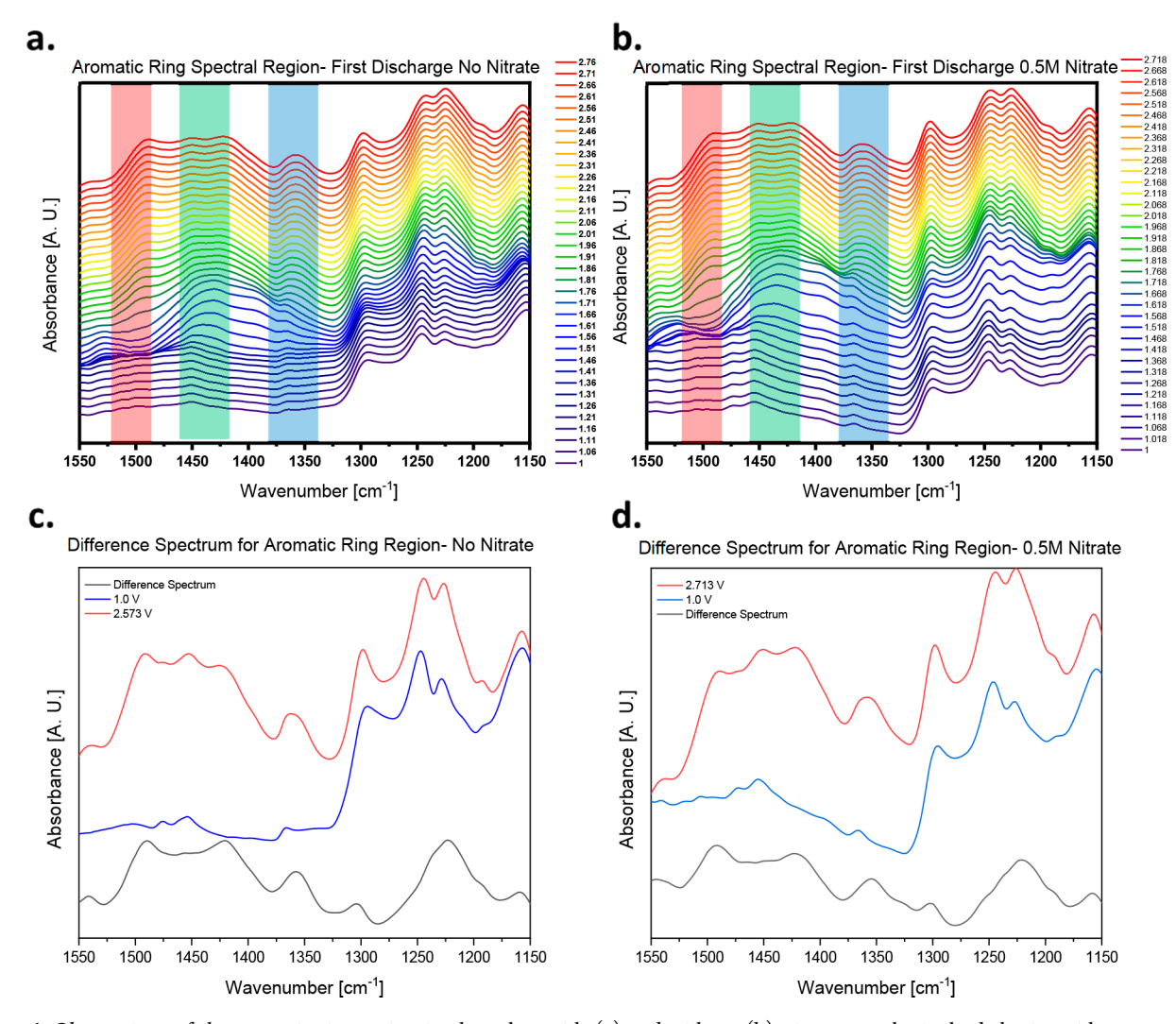


Figure 6. Observations of the aromatic ring region in electrolyte with (a) and without (b) nitrate reveals similar behavior with respect to the breakdown of several peaks in the spectral region due to Li^+ insertion. The peaks in question can be more clearly seen in the difference spectra between the OCV and full discharge for cells with and without lithium nitrate (c, d).

systems diverges. Cells without nitrate continue to exhibit LiPS signals (Figure 5c), albeit only short-chain LiPSs, while cells with nitrate demonstrate a distinct lack of clear LiPS peaks (Figure 5d). This is indicative of a process that occurs at the end of the first discharge, playing an important role in LiPS suppression. During the subsequent discharge cycle, no polysulfides are observed in the electrolyte with nitrate, demonstrating that effective polysulfide mitigation has been achieved. The same cannot be said for the electrolyte without nitrate as short-chain polysulfides (\sim 480–490 cm $^{-1}$) persist in the battery in the charged state, disappearing only after deeply discharging to <1.6 V. The difference between the two system can be observed in stark contrast in Figure S3, which highlights the persistence of short-chain polysulfides in the system without nitrate. Reobserving the CVs, the polysulfide peak for lower order polysulfides is far more prominent in cycles after the initial for electrolyte without nitrate. This could lend itself to much stronger IR absorption in comparison to that of the less prominent longer chain polysulfides.

Importantly, as we try to understand the mechanism behind lithium nitrate's ability to enable more stable cycling, we see the absence of polysulfides in the cell with nitrate. The presence of a CEI layer, coupled with the lack of polysulfides,

and the single-plateau behavior during cycling lead us to propose that a quasi-solid-state conversion process takes place in the Li-SPAN battery when electrolyte with nitrate is used. Single-plateau behavior is a hallmark of solid-solid conversion taking place.³⁴ Such conversion mechanisms have been proposed for SPAN batteries utilizing carbonate electrolytes, with ex-situ studies using XPS, XRF, and XANES proposing mechanisms involving the reaction of loose sulfur with carbonate electrolytes via nucleophilic attack leading to the formation of a CEI during the initial cycle.2,15,16 Enabling quasi-solid-state behavior in ether-based electrolytes has been demonstrated using in-operando XRD by Nazar et al. by tuning the solvation structure of the electrolyte.³⁵ Herein we propose that the presence of a robust CEI coupled with the formation and reformation of the C-S bond allows sulfur to exhibit solid-solid conversion characteristics in ether electrolytes. To the best of our knowledge, this is the first in-operando IR work that observes evidence of a quasi-solid-state conversion mechanism. Despite being unstable during the charge-discharge cycle, since we observe the degradation of the C-S bond in the in-situ spectra of SPAN only at <1.7 V, the C-S bond must still play an important role. The voltages required for sulfur reduction are higher (2.3-2.1 V) than those

required for C-S cleavage, and so the C-S bond must still anchor some portion of the sulfur and acts as a key aspect of sulfur entrapment.

In-Situ IR Observation of the Ring Structure. The lithiation of the cyclized polyacrylonitrile ring structure can also be observed using IR. During synthesis, aromatic ring structures form via dehydrogenation of the PAN backbone. As seen in Figure 6, this aromatic ring is visible via IR and can be seen in the 1550-1150 cm⁻¹ region. During discharge, as shown in Figure 6, we find that the 1360 and 1490 cm⁻¹ peaks in this region completely disappear. The insertion of an ionic species such as Li+ into any of these bonds is expected to disrupt the conjugated π structure associated with this ring and lead to the disruption of the associated bond vibrations. Analysis conducted on spectra taken during subsequent charge cycles finds that this region never recovers to its original state. To ensure the peaks had not been subsumed in the general absorbance increase of the electrolyte solution during discharge, Fourier self-deconvolution was performed on the charged and discharged spectra to enhance peak resolution, which confirmed that no new peaks had arisen in the aromatic region (Figure S2). Baseline absorbance increases were most likely due to volumetric changes during cycling of the cell. Increases in volume as discharge occurred due to the lower density of lithium sulfide increased pressure and allowed for a higher degree of contact between the cathode and the ATR crystal. Previous work using DFT has shown that lithiation of the SPAN backbone should occur. 18,26 Said study by Wang et al. also performed Li NMR studies that proposed the preferential interaction of lithium with the nitrogen atoms of the polymer backbone.²⁶ Unfortunately, due to the limitations of this technique, the exact location of the interaction cannot be confirmed other than its disruption of the conjugated π structure in the heterocyclic ring. Additionally, we can posit that the lithiation of the ring structure contributes to the large initial capacities seen in the first cycle. The lithiation of the SPAN polymer backbone plays an important role in the performance of SPAN, either via increases in conductivity or by providing a readily available source of lithium for the confined sulfur molecules and preventing full solvation from occurring.

CONCLUSION

In summary, we have investigated the electrochemical behavior of sulfurized polyacrylonitrile in ether electrolytes using operando FTIR. To the best of our knowledge, despite the intense focus this material has garnered in recent years, this is the first study that uses operando FTIR to study SPAN. We demonstrated that the use of high concentrations of lithium nitrate in ether electrolytes forms a cathode-electrolyte interface with high concentrations of lithium fluoride. This interface allows for more stable cycling in ether electrolytes, a phenomenon that was probed via in-operando FTIR. The inoperando studies revealed that ether electrolytes that contain a high concentration of lithium nitrate possess a C-S bond visible in the IR spectrum at 670 cm⁻¹ that reforms during cycling despite breaking in the initial cycle. This reformation process does not occur in electrolytes without lithium nitrate. Additionally, it is seen that soluble polysulfide species arise in both systems at ~500 cm⁻¹ during the first discharge but only persist in electrolytes without nitrate. This phenomenon coupled with the single-plateau behavior seen in the electrochemical tests leads us to believe that a quasi-solid-solid

reduction of sulfur occurs in electrolytes with nitrate. Such a transformation is enabled by a robust CEI coupled with a C–S bond that reforms during cycling. Additionally, we observed that the aromatic heterocyclic ring of the SPAN polymeric backbone lithiates during the first discharge. This lithiation allows for a convenient source of lithium ions during the subsequent reductions of sulfur. Overall, a mechanism via which stable cycling of SPAN in ether electrolytes with high concentrations of LiNO₃ is presented, enabled in part by CEI formation, C–S anchoring, and a quasi-solid-state reduction pathway.

ASSOCIATED CONTENT

Supporting Information

The Supporting Information is available free of charge at https://pubs.acs.org/doi/10.1021/acs.jpcc.3c03421.

Fourier self-deconvolution graphs of the aromatic ring region, select IR spectra that further highlights aspects of chemical transformation taking place, results of elemental analysis of the synthesized material, postmortem images of coin cells, and S 2p, O 1s, and C 1s XPS spectra (PDF)

AUTHOR INFORMATION

Corresponding Author

Vibha Kalra — Chemical and Biological Engineering, Drexel University, Philadelphia, Pennsylvania 19104, United States; orcid.org/0000-0002-2630-1560; Email: vk99@drexel.edu

Authors

Rhyz Pereira — Chemical and Biological Engineering, Drexel University, Philadelphia, Pennsylvania 19104, United States Krishna Kumar Sarode — Chemical and Biological Engineering, Drexel University, Philadelphia, Pennsylvania 19104, United States

Ayda Rafie — Chemical and Biological Engineering, Drexel University, Philadelphia, Pennsylvania 19104, United States Aaron Fafarman — Chemical and Biological Engineering, Drexel University, Philadelphia, Pennsylvania 19104, United

Complete contact information is available at: https://pubs.acs.org/10.1021/acs.jpcc.3c03421

Funding

This research was funded by the National Science Foundation under Awards NSF-2211049 and NSF-1938787.

Notes

ı

The authors declare no competing financial interest.

ACKNOWLEDGMENTS

The authors acknowledge the Materials Characterization Core at Drexel University for their aid in XPS collection.

REFERENCES

- (1) Manthiram, A.; Fu, Y.; Chung, S.-H.; Zu, C.; Su, Y.-S. Rechargeable Lithium-Sulfur Batteries. *Chem. Rev.* **2014**, *114* (23), 11751–11787.
- (2) Wu, Z.; Bak, S.-M.; Shadike, Z.; Yu, S.; Hu, E.; Xing, X.; Du, Y.; Yang, X.-Q.; Liu, H.; Liu, P. Understanding the Roles of the Electrode/Electrolyte Interface for Enabling Stable Li||Sulfurized

- Polyacrylonitrile Batteries. ACS Appl. Mater. Interfaces 2021, 13 (27), 31733–31740.
- (3) Zhang, S. S. Liquid electrolyte lithium/sulfur battery: Fundamental chemistry, problems, and solutions. *J. Power Sources* **2013**, 231, 153–162.
- (4) Seh, Z. W.; Sun, Y.; Zhang, Q.; Cui, Y. Designing high-energy lithium-sulfur batteries. *Chem. Soc. Rev.* **2016**, 45 (20), 5605–5634.
- (5) Cao, R.; Xu, W.; Lv, D.; Xiao, J.; Zhang, J.-G. Anodes for Rechargeable Lithium-Sulfur Batteries. *Adv. Energy Mater.* **2015**, *5* (16), 1402273.
- (6) Wild, M.; O'Neill, L.; Zhang, T.; Purkayastha, R.; Minton, G.; Marinescu, M.; Offer, G. J. Lithium sulfur batteries, a mechanistic review. *Energy Environ. Sci.* **2015**, 8 (12), 3477–3494.
- (7) Markevich, E.; Salitra, G.; Talyosef, Y.; Chesneau, F.; Aurbach, D. Review—On the Mechanism of Quasi-Solid-State Lithiation of Sulfur Encapsulated in Microporous Carbons: Is the Existence of Small Sulfur Molecules Necessary? *J. Electrochem. Soc.* **2017**, *164* (1), A6244—A6253.
- (8) Yim, T.; Park, M.-S.; Yu, J.-S.; Kim, K. J.; Im, K. Y.; Kim, J.-H.; Jeong, G.; Jo, Y. N.; Woo, S.-G.; Kang, K. S.; Lee, I.; Kim, Y.-J. Effect of chemical reactivity of polysulfide toward carbonate-based electrolyte on the electrochemical performance of Li-S batteries. *Electrochim. Acta* 2013, 107, 454–460.
- (9) Suo, L.; Hu, Y.-S.; Li, H.; Armand, M.; Chen, L. A new class of Solvent-in-Salt electrolyte for high-energy rechargeable metallic lithium batteries. *Nat. Commun.* **2013**, *4* (1), 1481.
- (10) Dörfler, S.; Althues, H.; Härtel, P.; Abendroth, T.; Schumm, B.; Kaskel, S. Challenges and Key Parameters of Lithium-Sulfur Batteries on Pouch Cell Level. *Joule* **2020**, *4* (3), 539–554.
- (11) Aurbach, D. Review of selected electrode-solution interactions which determine the performance of Li and Li ion batteries. *J. Power Sources* **2000**, *89* (2), 206–218.
- (12) Huang, C.-J.; Cheng, J.-H.; Su, W.-N.; Partovi-Azar, P.; Kuo, L.-Y.; Tsai, M.-C.; Lin, M.-H.; Panahian Jand, S.; Chan, T.-S.; Wu, N.-L.; Kaghazchi, P.; Dai, H.; Bieker, P. M.; Hwang, B.-J. Origin of shuttle-free sulfurized polyacrylonitrile in lithium-sulfur batteries. *J. Power Sources* **2021**, 492, 229508.
- (13) Wang, K.; Zhao, T.; Zhang, N.; Feng, T.; Li, L.; Wu, F.; Chen, R. Powering lithium-sulfur batteries by ultrathin sulfurized polyacrylonitrile nanosheets. *Nanoscale* **2021**, *13* (39), 16690–16695.
- (14) Langrud, S.; Razzaq, A. A.; Santhanagopalan, S.; Brow, R.; Xing, W. Comprehensive Characterization of Multi-Phase Sulfurized Polyacrylonitrile Cathodes for Lithium-Sulfur Batteries. *J. Electrochem. Soc.* **2022**, *169* (7), 070514.
- (15) Xing, X.; Li, Y.; Wang, X.; Petrova, V.; Liu, H.; Liu, P. Cathode electrolyte interface enabling stable Li-S batteries. *Energy Storage Materials* **2019**, 21, 474–480.
- (16) Rafie, A.; Kim, J. W.; Sarode, K. K.; Kalra, V. A review on the use of carbonate-based electrolytes in Li-S batteries: A comprehensive approach enabling solid-solid direct conversion reaction. *Energy Storage Materials* **2022**, *50*, 197–224.
- (17) Rehman, S.; Khan, K.; Zhao, Y.; Hou, Y. Nanostructured cathode materials for lithium-sulfur batteries: progress, challenges and perspectives. *J. Mater. Chem. A* **2017**, *5* (7), 3014–3038.
- (18) Jin, Z.-Q.; Liu, Y.-G.; Wang, W.-K.; Wang, A.-B.; Hu, B.-W.; Shen, M.; Gao, T.; Zhao, P.-C.; Yang, Y.-S. A new insight into the lithium storage mechanism of sulfurized polyacrylonitrile with no soluble intermediates. *Energy Storage Materials* **2018**, *14*, 272–278.
- (19) Wang, L.; He, X.; Sun, W.; Li, J.; Gao, J.; Tian, G.; Wang, J.; Fan, S. Organic polymer material with a multi-electron process redox reaction: towards ultra-high reversible lithium storage capacity. *RSC Adv.* **2013**, 3 (10), 3227–3231.
- (20) Zhang, S. S. Understanding of Sulfurized Polyacrylonitrile for Superior Performance Lithium/Sulfur Battery. *Energies* **2014**, *7* (7), 4588–4600.
- (21) Yu, X.-g.; Xie, J.-y.; Yang, J.; Huang, H.-j.; Wang, K.; Wen, Z.-S. Lithium storage in conductive sulfur-containing polymers. *J. Electroanal. Chem.* **2004**, *573* (1), 121–128.

- (22) Huang, X.; Liu, J.; Huang, Z.; Ke, X.; Liu, L.; Wang, N.; Liu, J.; Guo, Z.; Yang, Y.; Shi, Z. Flexible free-standing sulfurized polyacrylonitrile electrode for stable Li/Na storage. *Electrochim. Acta* **2020**, 333, 135493.
- (23) Fanous, J.; Wegner, M.; Grimminger, J.; Andresen, Ä.; Buchmeiser, M. R. Structure-Related Electrochemistry of Sulfur-Poly(acrylonitrile) Composite Cathode Materials for Rechargeable Lithium Batteries. *Chem. Mater.* **2011**, 23 (22), 5024–5028.
- (24) Rafie, A.; Pereira, R.; Shamsabadi, A. A.; Kalra, V. In Operando FTIR Study on the Effect of Sulfur Chain Length in Sulfur Copolymer-Based Li-S Batteries. *J. Phys. Chem. C* **2022**, *126* (30), 12327–12338.
- (25) Wang, X.; Qian, Y.; Wang, L.; Yang, H.; Li, H.; Zhao, Y.; Liu, T. Sulfurized Polyacrylonitrile Cathodes with High Compatibility in Both Ether and Carbonate Electrolytes for Ultrastable Lithium-Sulfur Batteries. *Adv. Funct. Mater.* **2019**, 29 (39), 1902929.
- (26) Wang, W.; Cao, Z.; Elia, G. A.; Wu, Y.; Wahyudi, W.; Abou-Hamad, E.; Emwas, A.-H.; Cavallo, L.; Li, L.-J.; Ming, J. Recognizing the Mechanism of Sulfurized Polyacrylonitrile Cathode Materials for Li-S Batteries and beyond in Al-S Batteries. *ACS Energy Lett.* **2018**, 3 (12), 2899–2907.
- (27) Yang, H.; Chen, J.; Yang, J.; Wang, J. Prospect of Sulfurized Pyrolyzed Poly(acrylonitrile) (S@pPAN) Cathode Materials for Rechargeable Lithium Batteries. *Angew. Chem., Int. Ed.* **2020**, 59 (19), 7306–7318.
- (28) Wei, S.; Ma, L.; Hendrickson, K. E.; Tu, Z.; Archer, L. A. Metal-Sulfur Battery Cathodes Based on PAN-Sulfur Composites. *J. Am. Chem. Soc.* **2015**, *137* (37), 12143–12152.
- (29) Li, W.; Yao, H.; Yan, K.; Zheng, G.; Liang, Z.; Chiang, Y.-M.; Cui, Y. The synergetic effect of lithium polysulfide and lithium nitrate to prevent lithium dendrite growth. *Nat. Commun.* **2015**, *6* (1), 7436.
- (30) Cheng, X.-B.; Yan, C.; Chen, X.; Guan, C.; Huang, J.-Q.; Peng, H.-J.; Zhang, R.; Yang, S.-T.; Zhang, Q. Implantable Solid Electrolyte Interphase in Lithium-Metal Batteries. *Chem.* **2017**, 2 (2), 258–270.
- (31) Qin, F.; Zhang, K.; Hong, B.; Zhang, L.; Zhang, Z.; Li, J.; Wang, X.; Lai, Y. A new insight into capacity fading of sulfurized polyacrylonitrile composite in carbonate electrolyte. *J. Electroanal. Chem.* **2021**, 882, 114964.
- (32) Wang, J.; Yang, J.; Wan, C.; Du, K.; Xie, J.; Xu, N. Sulfur Composite Cathode Materials for Rechargeable Lithium Batteries. *Adv. Funct. Mater.* **2003**, 13 (6), 487–492.
- (33) Dillard, C.; Singh, A.; Kalra, V. Polysulfide Speciation and Electrolyte Interactions in Lithium-Sulfur Batteries with in Situ Infrared Spectroelectrochemistry. *J. Phys. Chem. C* **2018**, *122* (32), 18195–18203.
- (34) Han, F.; Yue, J.; Fan, X.; Gao, T.; Luo, C.; Ma, Z.; Suo, L.; Wang, C. High-Performance All-Solid-State Lithium-Sulfur Battery Enabled by a Mixed-Conductive Li2S Nanocomposite. *Nano Lett.* **2016**, *16* (7), 4521–4527.
- (35) Pang, Q.; Shyamsunder, A.; Narayanan, B.; Kwok, C. Y.; Curtiss, L. A.; Nazar, L. F. Tuning the electrolyte network structure to invoke quasi-solid state sulfur conversion and suppress lithium dendrite formation in Li-S batteries. *Nature Energy* **2018**, 3 (9), 783–791.